

**Modulating drift dynamics of circle swimmers by periodic potentials**Mohammad Nabil,<sup>1,2</sup> Andrew Frankowski,<sup>1,2,\*</sup> Ashton Orosa,<sup>1,2,\*</sup> Andrew Fuller,<sup>1,2,\*</sup> and Amir Nourhani<sup>1,2,3,†</sup><sup>1</sup>*Department of Mechanical Engineering, University of Akron, Akron, Ohio 44325, USA*<sup>2</sup>*Biomimicry Research and Innovation Center, University of Akron, Akron, Ohio 44325, USA*<sup>3</sup>*Departments of Biology, Mathematics, and Chemical, Biomolecular, and Corrosion Engineering, University of Akron, Akron, Ohio 44325, USA*

(Received 6 March 2022; accepted 22 April 2022; published 31 May 2022)

We propose a method to modulate the drifting motion of overdamped circle swimmers in steady fluid flows by means of static sinusoidal potentials. Using Langevin formalism, we study drift velocity as a function of potential strength and wavelength with and without diffusional motion. Drift velocity is essentially quantized without diffusion, but in the presence of noise, the displacement per cycle has a continuous range. As a function of dimensionless potential wave number, domains of damped oscillatory and plateau regimes are observed in the drift velocity diagram. At weak potential and fluid velocity less than powered velocity, there is also a regime where drift velocity exceeds the fluid velocity. Methods based on these results can be used to separate biological and artificial circle swimmers based on their dynamical properties.

DOI: [10.1103/PhysRevE.105.054610](https://doi.org/10.1103/PhysRevE.105.054610)**I. INTRODUCTION**

Active microswimmers, which generate motion by harvesting energy from their environment, have been the subject of intense research both at fundamental and applied levels [1]. The desire to exploit these microswimmers for microscale manipulations of both single-particle and collective dynamics has led to proof-of-concept examples for smart microrobots [1], multipart active self-assemblies [2], biomedical [3–6], environmental remediation [7–10], cargo carrying [11–14], or contactless pushing [15] applications. Controlling the motion of these particles is of paramount importance to exploit them for targeted applications.

In this paper, we combine fluid flow with one-dimensional background potential to modulate the drifting motion of circle swimmers in a fluid. Circle swimmers, also known as chiral active particles, are a class of microscale self-propellers which, due to structural asymmetry, follow circular trajectories [16] in the absence of noise [17] or any obstacles along their paths [18,19] instead of straight paths. The propulsive mechanism is abstracted away in our model, which should therefore be applicable to stroke-based dynamics [20] as well as self-phoretic propulsion [21]. We thus use the word swimmer in a neutral sense. A Brownian circle swimmer undergoing stochastic orientational dynamics superposed on its deterministic powered rotary motion follows a curved trajectory [22–24].

From a practical perspective, one may see two challenges impeding the exploitation of rotary active particles for useful applications in complex environments. One is controlling their motion and the other is separating these particles based on their dynamical properties. Controlling the dynamics of active

particles is usually done through interaction with external field [25] or background potential [26–29], particle-particle interactions [15,30–34], and interactions with boundaries [22,35] or hard obstacles [36–41]. Several techniques have been used to separate circle swimmers, including motion in a patterned substrate with L-shaped obstacles [18], chiral flowers [19], rotary obstacles [42], or motion under a two-dimensional background potential [26,27].

In our paper, we exploit a one-dimensional sinusoidal standing wave [26] as one of the simplest potential fields that can be applied to a swimmer in a fluid. To break the symmetry when powered motion dominates the noise [17] and opens the circular trajectory, a flow field is applied parallel to the wave vector of the potential (see Fig. 1). Depending on the properties of the microswimmer, fluid velocity, and properties of the wave (such as amplitude and wavelength), the microrobot's drift velocity can be controlled within a reasonable range.

In the negligible-noise regime, we find that, for a given potential strength, the drift velocity as a function of potential finesse consists of a set of discrete curves. With the introduction of noise, these curves turn into a continuous curve consisting of a damped oscillatory section and a plateau part. We present the results in the form of a phase diagram that

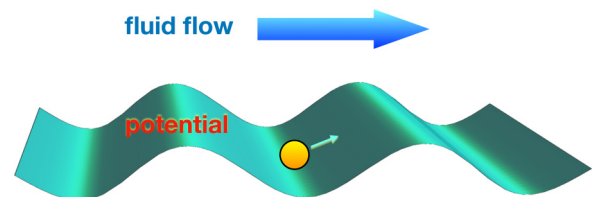


FIG. 1. Schematic of the setup: A circle microswimmer is drifted by fluid flow and its motion is modulated by a sinusoidal background potential. The direction of the fluid flow is along the wave vector of the potential.

\*These authors contributed equally to this work.

†nourhani@uakron.edu

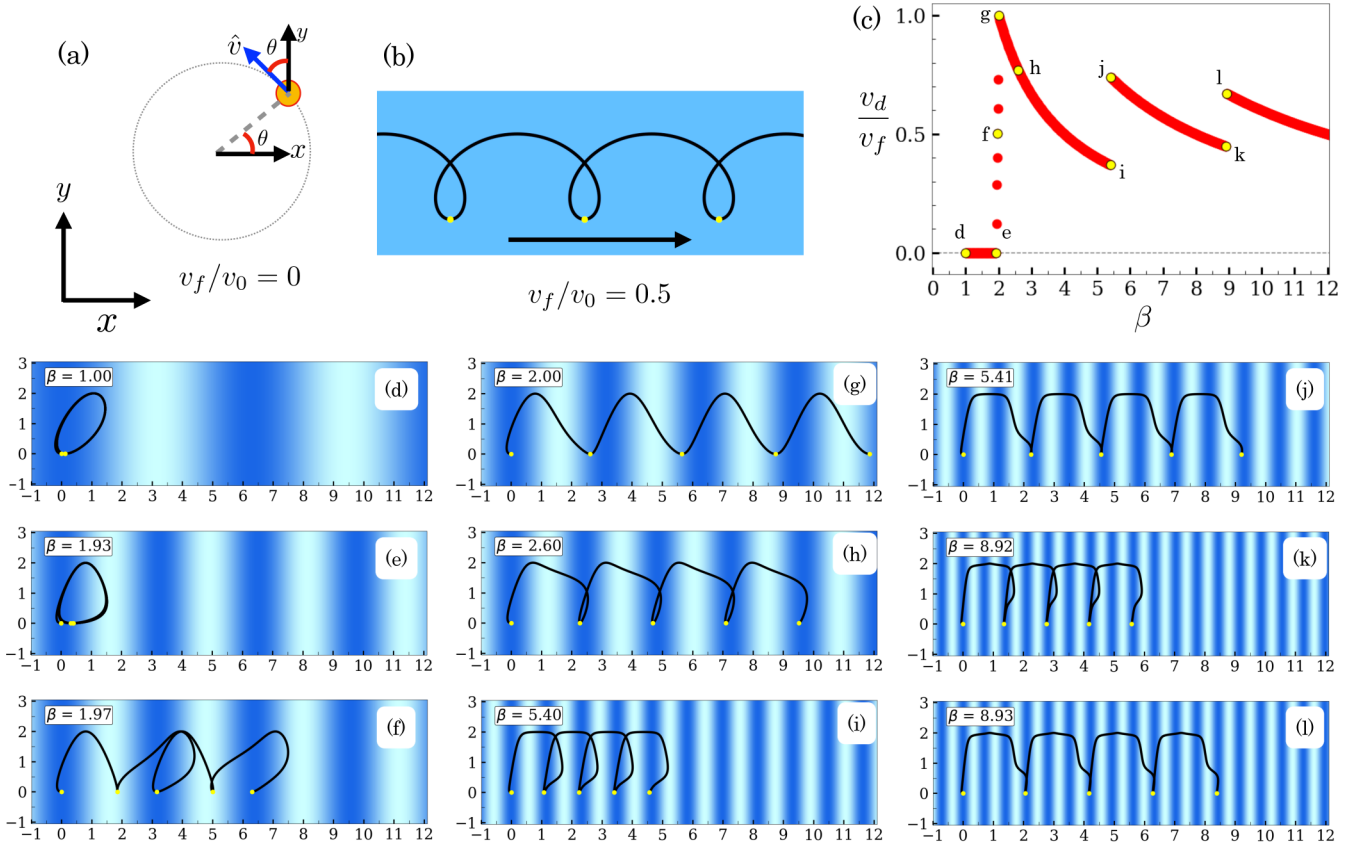


FIG. 2. (a) A rotary active particle with rectilinear  $v_0$  and angular  $\omega$  speeds follows a circular trajectory in the absence of noise and an external field. (b) Addition of a flow field opens the circular path into a cyclic trajectory and the particle drifts with the fluid. (c) Drift velocity  $v_d$  relative to fluid velocity  $v_f$  as a function of finesse  $\beta$  with resolution  $\Delta\beta = 0.01$  for  $\alpha = 1$  and relative fluid velocity  $v_f/v_0 = 0.5$ . The marks  $d-l$  on the graph represent the trajectories in the absence of noise and in the presence of background potential with  $\alpha = 1$  and finesse  $\beta$  equal to (d) 1.00, (e) 1.94, (f) 1.97, (g) 2.00, (h) 2.60, (i) 5.40, (j) 5.41, (k) 8.92, (l) 8.93. The dark areas are minima of the potential, and the light are maxima. The yellow dots in each figure show the beginning or end of a full cycle in a particle trajectory.

shows the drift velocity relative to fluid velocity as a function of dimensionless potential strength and fluid velocity in the plateau regime. The potential application for this research could lead to modulating the drifting motion and sorting biological [43–48] and artificial [49–53] circle swimmers based on their dynamical properties.

## II. PROBLEM FORMULATION

In the absence of a potential, a rotary swimmer moves in a fluid near a surface ( $xy$  plane) with velocity  $\mathbf{v} = v_0 \hat{v}$ , where  $v_0$  is the powered speed and  $\hat{v}$  is the swimmer's intrinsic orientation. The active particle rotates with an angular velocity  $s_\omega \omega$  with  $\omega > 0$ . Clockwise ( $s_\omega = -1$ ) rotation can be changed to counterclockwise ( $s_\omega = +1$ ) by a reflection about the  $x$  axis which changes nothing else, so the two cases must have the same drift velocity. Therefore, we focus on the former without loss. The chirality of the swimmer is stable and remains unchanged. A background fluid flow with velocity  $\mathbf{v}_f = v_f \hat{x}$  further translates the self-propeller in the  $\hat{x}$  direction. Under overdamped dynamics, a static one-dimensional external potential  $V(\mathbf{r})$  supplies an additive velocity contribution  $-\mu \nabla V$ , where  $\mu$  is the Stokes mobility of the swimmer.

The combination of powered motion, background fluid flow, and spatially periodic potential governs the deterministic

dynamics of the swimmer and the instantaneous velocity is no longer in the direction of the intrinsic orientation. The one-dimensional potential is a standing wave  $\mu V(\mathbf{r}) = C \cos(K\hat{x} \cdot \mathbf{r})$  of amplitude  $C/\mu$  and wavelength  $\lambda = 2\pi/K$ . From these quantities, we can create dimensionless strength and finesse parameters [26]

$$\alpha = \frac{CK}{v_0}, \quad \beta = \frac{Kv_0}{\omega} = KR, \quad (1)$$

respectively, where  $R = v_0/\omega$  is the free swimmer orbit radius due to the powered motion in the absence of noise, fluid flow, and periodic potential. Working in units of  $\omega^{-1}$  for time and  $R$  for length and taking into account the orientational and translational diffusions, the overdamped motion of the particle is governed by the Langevin equations

$$\begin{aligned} \frac{d\mathbf{r}}{dt} &= \hat{v}(\theta(t)) + \frac{v_f}{v_0} \hat{x} + \alpha \sin(\beta \hat{x} \cdot \mathbf{r}) \hat{x} + \boldsymbol{\xi}(t), \\ \frac{d\theta}{dt} &= s_\omega + \zeta(t), \end{aligned} \quad (2)$$

where, as shown in Fig. 2(a),  $\theta$  is the angle the intrinsic orientation makes with the  $s_\omega \hat{y}$  direction, and  $s_\omega \hat{v}(\theta) = -\sin(\theta) \hat{x} + \cos(\theta) \hat{y}$ . The two-dimensional zero-mean white noise  $\boldsymbol{\xi}$  has dimensionless strength  $\gamma_t = D_t \omega / v_0^2$  for passive translational diffusion and the one-dimensional zero mean

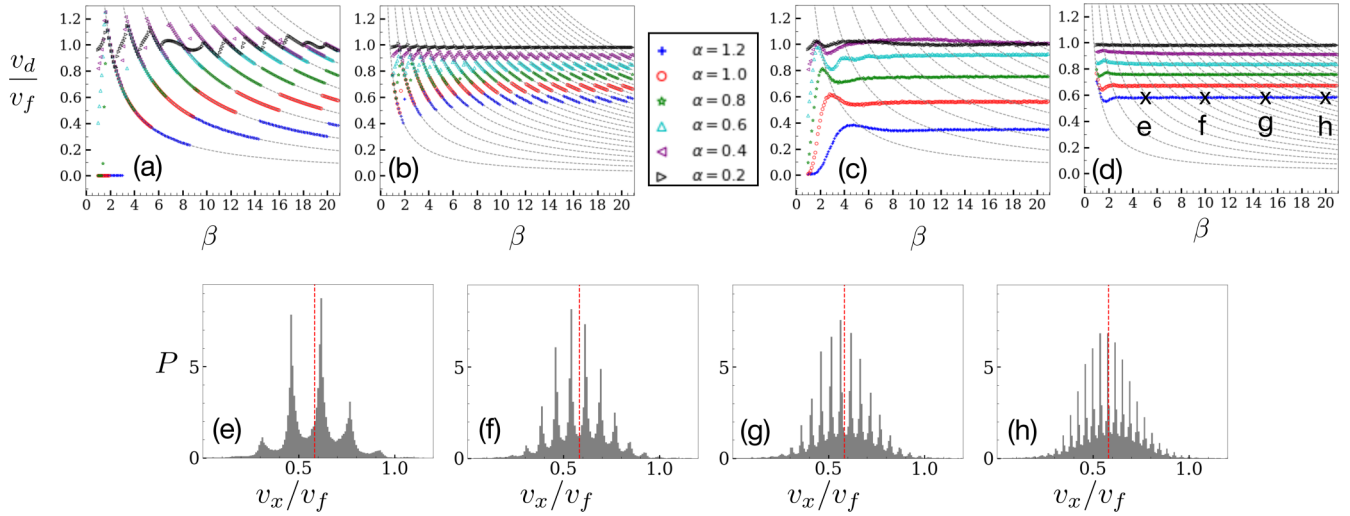


FIG. 3. Drift velocity  $v_d$  relative to fluid velocity  $v_f$  as a function of  $\beta$  with resolution  $\Delta\beta = 0.1$  for different values of  $\alpha$  for parameter pairs  $(v_f/v_0, \gamma_o)$  of (a) (0.5, 0), (b) (1.3, 0), (c) (0.5, 0.1), and (d) (1.3, 0.1). Dashed gray lines are theoretical curves according to Eq. (3) for different values of  $n$ . (e)–(h) Histograms of  $x$  displacement over a single rotational period  $T$  relative to fluid velocity  $v_f$  for points marked on (d) for  $\alpha = 1.2$ . The dashed red lines show the drift velocity. The tall peaks in the histograms represent the minima of the potential where the particle tends to end up after each cycle.

white noise  $\zeta$  with dimensionless strength  $\gamma_o = D_o/\omega$  accounts for orientational diffusion.  $D_t$  and  $D_o$  are conventional translational and orientational diffusion coefficients, respectively.

We ran the simulation for three values of fluid velocity  $v_f = 0.5v_0, 0.9v_0$ , and  $1.3v_0$ , six values of dimensionless potential strength  $\alpha = 0.2, 0.4, 0.6, 0.8, 1.0$ , and  $1.2$ , in the finesse range  $1 \leq \beta \leq 20$ . The deterministic simulations (no noise) were run for 100 periods of rotations with time steps  $\Delta t = T/3600$ . The drift speed is calculated from displacement over the last 95 rotational periods, since the trajectories are found to fall very close to the trajectory attractor after only one period except in the transition regions. For simulations with noise, for each pair of  $\alpha$  and  $\beta$  we ran the simulations for 1000 rotational periods and we used the last 995 periods to calculate the average drift speed shown in Fig. 3 and Figs. S2 and S3 of the Supplemental Material [54].

We chose the one-dimensional white noise values  $\gamma_o = 0.01$  and  $0.1$  based off experimental data [50–52] showing that a typical artificial swimmer has values  $0.009 \lesssim \gamma_o \lesssim 0.05$  [16]. For a swimmer to behave like a circle swimmer, angular speed  $\omega$  should be more than the orientational diffusivity  $D_o$  so the swimmer can rotate and move along a significant portion of the circular trajectory before its orientation is distorted by the stochastic noise. Therefore,  $\gamma_o$  should be less than one. As shown in Fig. S1 in the Supplemental Material [54], our chosen values for  $\gamma_o$  produce similar patterns of damped oscillation at small values of  $\beta$  and a plateau regime at higher values of  $\beta$ . For demonstration, we show the results for  $\gamma_o = 0.1$  in Figs. 3(c) and 3(d). Also, for translational noise we have  $0.005 \lesssim \gamma_t \lesssim 0.02$  [16] and we picked  $\gamma_t = 0.001$  and  $0.01$  for our simulations. As shown in Fig. S3 in the Supplemental Material [54], the translational noise has similar effects to orientational noise and in the main text we focus on the effect of orientational diffusivity in Fig. 3.

### III. RESULTS AND DISCUSSION

In what follows, we discuss the dynamics of the circle swimmer in the noise-negligible regime and provide a simple theory to explain the observations. Then, we add the effect of noise to our system and investigate how it influences the deterministic behavior.

#### A. Deterministic dynamics

We start our analysis with purely deterministic dynamics of a circle swimmer as a result of its powered motion [Fig. 2(a)] in the absence of noise where the state of the swimmer on its trajectory is identified by  $\theta$ . Addition of fluid flow with velocity  $v_f \hat{x}$  opens the circular trajectory and the microswimmer displaces with drift speed  $v_d$  equal to the fluid speed  $v_f$  [Fig. 2(b)]. Adding the potential, however, causes the drift velocity to deviate from the fluid velocity  $v_f$ . The ratio  $v_d/v_f$  is a function of potential and microswimmer characteristics, the coupling of which is manifested in parameters  $\alpha$  and  $\beta$ .

The background potential influences the microswimmer drift in a controlled manner depending on values of  $\alpha$  and  $\beta$ . Figure 2(c) shows the drift velocity  $v_d$  relative to fluid velocity  $v_f$  for constant  $\alpha = 1$  as a function of finesse  $\beta$  in the form of a set of discrete curves such that the drift velocity jumps from one curve to the next at some transitions. The marked points in Fig. 2(c) correspond to nine graphs, Figs. 2(d)–2(l), showing the trajectory of the swimmer over four rotational cycles. The dark areas are minima and the light are the maxima of the potential. The transition in the trajectories from one curve to another with increasing  $\beta$  follows a shrink-expansion pattern. The videos in the Supplemental Material [54] show this phenomenon for  $v_f = 0.5v_0, 0.9v_0$ , and  $1.3v_0$  for various values of  $\alpha$ . With an increase in  $\beta$ , the trajectory shrinks before it is able to transition into a higher drift velocity. After each shrinking and subsequent expansion,

the swimmer does not reach as high a drift velocity as during the previous expansion. This is shown in Fig. 2(c), comparing the  $v_d/v_f$  of points  $g$ ,  $j$ , and  $l$ .

For constant  $\alpha = 1$  and small values of  $\beta \simeq 1$ , the open trajectory turns into a distorted circular trajectory and the particle is trapped inside the potential minimum. In the region  $\beta \lesssim 1.93$ , the average drift velocity of the particle is nearly zero. The particle is not able to pass the potential maxima. With even higher values of  $\beta$ , the distortion continues up to a point at which the trajectory passes the maximum of the potential and thus opens. Figure 2(f) is an example of a transition regime to an open trajectory where we see a repeating pattern with periodicity more than one  $T$ . Eventually, at  $\beta \simeq 2$ , the trajectory opens and extends in space.

With even further increase in  $\beta$ , the trajectory shrinks while during each period of powered motion the swimmer passes only one potential maximum. The trend continues up to the point [Fig. 2(i)] that with a small increase in  $\beta$  the trajectory is ready to pass two potential maxima [Fig. 2(j)]. Again, with still further increase in  $\beta$ , the trajectory shrinks and thus the drift velocity decreases, until we reach a state that part of the trajectory gets close to a potential maximum [Fig. 2(k)] and afterward the swimmer passes three maxima [Fig. 2(l)]. This pattern continues, with the swimmer skipping greater numbers of potential maxima as we increase  $\beta$ .

The transitions between discrete curves in Fig. 2(c) are the result of the change in the number of potential maxima a swimmer passes over one period of rotation. We observe that each curve has a dependance on  $\beta^{-1}$ . The reason is that a particle passes  $n$  maxima during one rotation period  $T = 2\pi/\omega$  and thus moves forward a distance of  $n\lambda = 2\pi n/K$ . Thus, the drift velocity  $v_d$  relative to fluid velocity  $v_0$  is

$$\frac{v_d}{v_f} = \frac{1}{v_f} n \frac{\lambda}{T} = n \frac{1}{v_f} \frac{\omega}{K} = n \frac{1}{v_f} \frac{R\omega}{\beta} = n \left( \frac{v_f}{v_0} \right)^{-1} \beta^{-1}, \quad (3)$$

which depends on the inverse of  $\beta$ , and  $\beta v_d$  can only take discrete values.

In addition to the potential finesse, both the potential strength and the fluid velocity influence the drift velocity of the circle swimmer. Figures 3(a) and 3(b) for  $v_f = 0.5v_0$  and  $1.3v_0$ , respectively, show the drift velocity for several values of  $\alpha$ . The average drift velocities for different values of  $\alpha$  and  $\beta$  tend to fall on a general set of curves (especially for high values of  $\alpha$ ) represented by the dashed gray curves showing theoretical values from Eq. (3) for distinct values of  $n$ . With an increase in  $\alpha$ , the drift velocity tends to decrease. As shown in Fig. 3(a) for small values of  $\alpha = 0.2$  and  $0.4$  and small values of fluid velocity  $v_f = 0.5v_0$ , the drift velocity curves show significant overlap. More importantly, in this regime the drift velocity can exceed the driving fluid velocity for some values of  $\beta$  (see Supplemental video [54] v05.m4v for demonstration of the corresponding trajectories). For high values of potential strength, the potential decreases the relative drift velocity, while for small values of potential strength the potential enhances the drift. As shown in Fig. 3(b), at values of fluid velocity  $v_f = 1.3v_0$  higher than the powered velocity  $v_0$ , the overlaps between the curves for different  $\alpha$  values

decrease significantly. Using these results, under the same periodic potential we can set the potential parameters such that particles with different dynamical properties can be separated. The supplemental video sep.m1v demonstrates the separation of two particles.

## B. Addition of stochastic dynamics

Noise at the microscale can be as strong as deterministic motion [16,55,56] and can have a significant effect on the dynamics of circle swimmers [23,57–59]. Correspondingly, the addition of noise to our system makes significant changes to drift velocity. Apart from some fluctuations for small values of  $\beta$ , the drift velocity is independent of  $\beta$ . In the regime of small  $\beta$ , parts of the drift velocity curves behave similarly to the deterministic dynamics and fall on the dashed theoretical curves according to Eq. (3). However, the transitions between the predicted theoretical states are continuous and we do not observe jumps between discrete curves as in the deterministic scenarios in Figs. 3(a) and 3(b). For example, as shown in Figs. 2(k) and 2(l), with a small change in  $\beta$  from 8.92 to 8.93, the trajectory significantly changes, but if we have a noise present, these two states can interchange easily. Therefore, the displacement is effectively an average over possible displacements near  $\beta = 8.92$ . The noise smooths the discontinuities seen in the deterministic plots. With an increase in fluid velocity, the domain of  $\beta$  over which we observe the plateau behavior increases.

Contrary to the deterministic scenario, where in each period the microswimmer passes a specific number of potential maxima, the introduction of noise leads to a continuous range of displacements during a cycle. The resulting drift velocity is an average over these displacements per cycle. In Fig. 3(d), for  $\alpha = 1.2$  and  $v_f/v_0 = 1.3$ , we have identified four points with  $\beta$  equal to 5 for  $f$ , 10 for  $g$ , 15 for  $h$ , and 20 for  $i$ . Their corresponding histograms for relative drift per cycle in the  $x$  direction,  $v_x/v_f$ , are plotted in Figs. 3(e)–3(h). The velocity in the  $x$  direction,  $v_x = \Delta x/T$ , is measured by dividing the displacement  $\Delta x$  after one period  $T$ .

In the histograms, the peaks correspond to displacements equal to multiples of the wavelength and suggest that the chance of a particle going into a local minimum after each cycle is high. The presence of multiple peaks shows that a swimmer passes different numbers of maxima at different cycles, but these numbers have a limited range. While these histograms are distinct for different values of  $\beta$ , the drift is almost the same and independent of  $\beta$ , because the drift velocity is the statistical average over the displacements. Within this framework, the histogram for a deterministic scenario would be a single peak delta function. The addition of the noise widens the distribution.

Figure 4 shows phase diagrams of the relative drift velocities  $v_d/v_0$  and  $v_d/v_f$  in the plateau regime as a function of dimensionless potential strength  $\alpha$  and relative fluid velocity  $v_f/v_0$  for  $\gamma_0 = 0.1$ . At small values of  $\alpha$ , the particle drifts with a velocity close to fluid velocity. In the regime of strong potential and small fluid velocity, the drift is very small. Figure 4(b) shows how to modulate and fine-tune the drift velocity as a fraction of fluid flow by changing the potential strength. We can differentiate and separate particles with

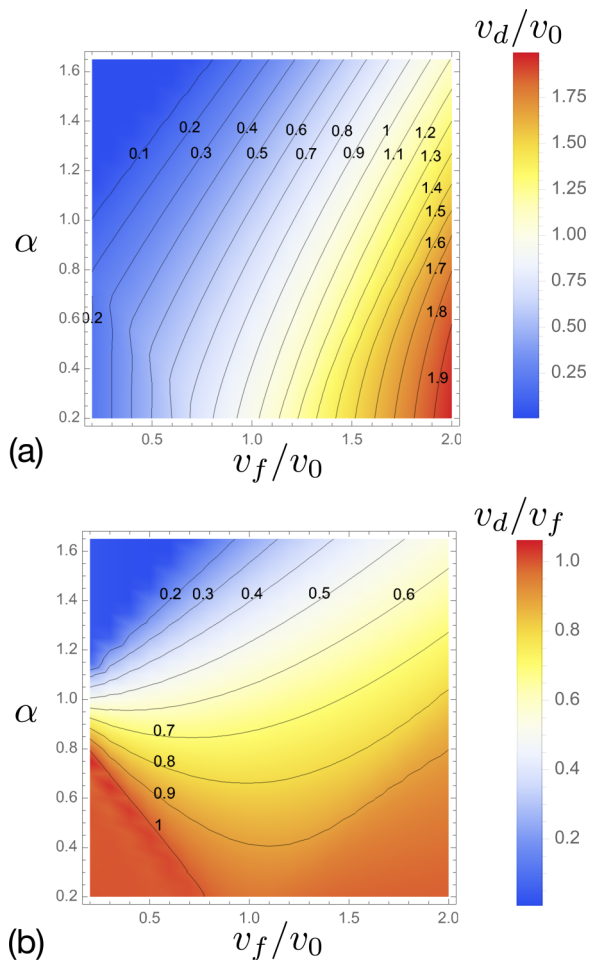


FIG. 4. The behavior in the  $\beta$ -independent regime for  $\gamma_0 = 0.1$ .

distinct dynamical properties (powered rectilinear speed  $v_0$  and angular velocity  $\omega$ ). In an experimental setup  $v_f$ ,  $C$ , and  $K$  (or  $\lambda$ ) are fixed. For a given Brownian circle swimmer, if  $v_0$  and  $\omega$  are such that  $\beta = v_0 K / \omega$  falls in the  $\beta$ -independent plateau regime, effectively only  $v_0$  through  $\alpha = CK/v_0$  contributes to the drift velocity, while if  $\beta$  falls in nonplateau regime, both  $\omega$  and  $v_0$  affect the drift velocity.

#### IV. CONCLUSION

We studied the drift motion of circle swimmers in a periodic potential using Langevin formalism. In the deterministic regime, the drift velocity as a function of potential finesse consists of a discrete set of curves. Each curve represents a set of trajectories along which the particle only passes a specific number of potential maxima. While increasing the potential finesse, the drift velocity hops between these curves moving toward passing a greater number of potential maxima per cycle. In the regime where noise has a significant effect on the dynamics, the discontinuous curves for a given potential strength become continuous with oscillations at small  $\beta$  and a plateau at larger values. By choosing appropriate potential parameters and fluid velocity, we can separate circle swimmers based on their rectilinear and angular velocities.

#### ACKNOWLEDGMENTS

This work was supported by funding from the University of Akron. We are grateful to Paul Lammert, Wei Wang, and Nathaniel Wentzel for their insightful comments and suggestions. A. Frankowski, A.O., and A. Fuller acknowledge funding from Undergraduate Research Opportunities Program through the Department of Mechanical Engineering at the University of Akron.

- [1] F. Soto, E. Karshalev, F. Zhang, B. Esteban Fernandez de Avila, A. Nourhani, and J. Wang, Smart materials for microrobots, *Chem. Rev.* **122**, 5365 (2022).
- [2] S. A. Nabavizadeh, J. Castañeda, J. G. Gibbs, and A. Nourhani, Gravitropically stabilized self-assembly of active microcrystallites and spinning free Janus particles, *Part. Part. Syst. Charact.* **39**, 2100232 (2022).
- [3] C. Gao, Y. Wang, Z. Ye, Z. Lin, X. Ma, and Q. He, Biomedical micro-/nanomotors: From overcoming biological barriers to in vivo imaging, *Adv. Mater.* **33**, 2000512 (2021).
- [4] J. Ou, K. Liu, J. Jiang, D. A. Wilson, L. Liu, F. Wang, S. Wang, Y. Tu, and F. Peng, Micro-/nanomotors toward biomedical applications: The recent progress in biocompatibility, *Small* **16**, 1906184 (2020).
- [5] M. Safdar, S. U. Khan, and J. Jänis, Progress toward catalytic micro- and nanomotors for biomedical and environmental applications, *Adv. Mater.* **30**, 1703660 (2018).
- [6] M. Wan, T. Li, H. Chen, C. Mao, and J. Shen, Biosafety, functionalities, and applications of biomedical micro/nanomotors, *Angew. Chem., Int. Ed.* **60**, 13158 (2021).
- [7] J. Parmar, D. Vilela, K. Villa, J. Wang, and S. Sanchez, Micro- and nanomotors as active environmental microcleaners and sensors, *J. Am. Chem. Soc.* **140**, 9317 (2018).
- [8] L. Soler and S. Sánchez, Catalytic nanomotors for environmental monitoring and water remediation, *Nanoscale* **6**, 7175 (2014).
- [9] M. Safdar, J. Simmchen, and J. Jänis, Light-driven micro- and nanomotors for environmental remediation, *Environ. Sci.: Nano* **4**, 1602 (2017).
- [10] M. Zarei and M. Zarei, Self-propelled micro/nanomotors for sensing and environmental remediation, *Small* **14**, 1800912 (2018).
- [11] X. Ma, K. Hahn, and S. Sanchez, Catalytic mesoporous Janus nanomotors for active cargo delivery, *J. Am. Chem. Soc.* **137**, 4976 (2015).
- [12] D. Xu, Y. Wang, C. Liang, Y. You, S. Sanchez, and X. Ma, Self-propelled micro/nanomotors for on-demand biomedical cargo transportation, *Small* **16**, 1902464 (2020).
- [13] S. Sundararajan, S. Sengupta, M. E. Ibele, and A. Sen, Drop-off of colloidal cargo transported by catalytic Pt-Au nanomotors via photochemical stimuli, *Small* **6**, 1479 (2010).
- [14] J. A. Tejada-Rodríguez, A. Nunez, F. Soto, V. García-Gradilla, R. Cadena-Nava, J. Wang, and R. Vazquez-Duhalt, Virus-based nanomotors for cargo delivery, *ChemNanoMat* **5**, 194 (2019).

- [15] A. Nourhani, D. Brown, N. Pletzer, and J. G. Gibbs, Engineering contactless particle–particle interactions in active microswimmers, *Adv. Mater.* **29**, 1703910 (2017).
- [16] A. Nourhani, Y.-M. Byun, P. E. Lammert, A. Borhan, and V. H. Crespi, Nanomotor mechanisms and motive force distributions from nanorotor trajectories, *Phys. Rev. E* **88**, 062317 (2013).
- [17] D. Ahmed, M. Lu, A. Nourhani, P. E. Lammert, Z. Stratton, H. S. Muddana, V. H. Crespi, and T. J. Huang, Selectively manipulable acoustic-powered microswimmers, *Sci. Rep.* **5**, 9744 (2015).
- [18] C. Reichhardt and C. O. Reichhardt, Dynamics and separation of circularly moving particles in asymmetrically patterned arrays, *Phys. Rev. E* **88**, 042306 (2013).
- [19] M. Mijalkov and G. Volpe, Sorting of chiral microswimmers, *Soft Matter* **9**, 6376 (2013).
- [20] R. Ledesma-Aguilar, H. Löwen, and J. M. Yeomans, A circle swimmer at low Reynolds number, *Eur. Phys. J. E* **35**, 70 (2012).
- [21] M. Nabil, S. A. Nabavizadeh, P. E. Lammert, and A. Nourhani, A spectral method for axisymmetric Stokes flow past a particle, *J. Fluid Mech.* **936**, R1 (2022).
- [22] S. van Teeffelen and H. Löwen, Dynamics of a Brownian circle swimmer, *Phys. Rev. E* **78**, 020101(R) (2008).
- [23] A. Nourhani, P. E. Lammert, A. Borhan, and V. H. Crespi, Chiral diffusion of rotary nanomotors, *Phys. Rev. E* **87**, 050301(R) (2013).
- [24] T. Jamali and A. Naji, Active fluids at circular boundaries: Swim pressure and anomalous droplet ripening, *Soft Matter* **14**, 4820 (2018).
- [25] F.-j. Lin, J.-j. Liao, and B.-q. Ai, Separation and alignment of chiral active particles in a rotational magnetic field, *J. Chem. Phys.* **152**, 224903 (2020).
- [26] A. Nourhani, V. H. Crespi, and P. E. Lammert, Guiding Chiral Self-Propellers in a Periodic Potential, *Phys. Rev. Lett.* **115**, 118101 (2015).
- [27] J.-c. Wu, J.-n. Zhou, and B.-q. Ai, Transport reversals of chiral active particles induced by a perpendicular constant force, *Physica A* **462**, 864 (2016).
- [28] H. Ribeiro, W. Ferreira, and F. Q. Potiguar, Trapping and sorting of active matter in a periodic background potential, *Phys. Rev. E* **101**, 032126 (2020).
- [29] S. Kumari, A. S. Nunes, N. A. Araújo, and M. M. Telo da Gama, Demixing of active particles in the presence of external fields, *J. Chem. Phys.* **147**, 174702 (2017).
- [30] J. N. Johnson, A. Nourhani, R. Peralta, C. McDonald, B. Thiesing, C. J. Mann, P. E. Lammert, and J. G. Gibbs, Dynamic stabilization of Janus sphere trans-dimers, *Phys. Rev. E* **95**, 042609 (2017).
- [31] B.-q. Ai, Z.-g. Shao, and W.-r. Zhong, Mixing and demixing of binary mixtures of polar chiral active particles, *Soft Matter* **14**, 4388 (2018).
- [32] S. Tang, F. Zhang, J. Zhao, W. Talaat, F. Soto, E. Karshalev, C. Chen, Z. Hu, X. Lu, J. Li *et al.*, Structure-dependent optical modulation of propulsion and collective behavior of acoustic/light-driven hybrid microbowls, *Adv. Funct. Mater.* **29**, 1809003 (2019).
- [33] C. Reichhardt and C. O. Reichhardt, Reversibility, pattern formation, and edge transport in active chiral and passive disk mixtures, *J. Chem. Phys.* **150**, 064905 (2019).
- [34] S. Jahanshahi, C. Lozano, B. Ten Hagen, C. Bechinger, and H. Löwen, Colloidal Brazil nut effect in microswimmer mixtures induced by motility contrast, *J. Chem. Phys.* **150**, 114902 (2019).
- [35] J.-l. Liu, S.-c. Lu, and B.-q. Ai, Ratchet transport of chiral particles caused by the transversal asymmetry: Current reversals and particle separation, *J. Phys. Soc. Jpn.* **87**, 064004 (2018).
- [36] G. Volpe, I. Buttinoni, D. Vogt, H.-J. Kümmerer, and C. Bechinger, Microswimmers in patterned environments, *Soft Matter* **7**, 8810 (2011).
- [37] A. Chamolly, T. Ishikawa, and E. Lauga, Active particles in periodic lattices, *New J. Phys.* **19**, 115001 (2017).
- [38] C. Reichhardt and C. Reichhardt, Clogging, dynamics, and reentrant fluid for active matter on periodic substrates, *Phys. Rev. E* **103**, 062603 (2021).
- [39] C. Reichhardt and C. Reichhardt, Active matter commensuration and frustration effects on periodic substrates, *Phys. Rev. E* **103**, 022602 (2021).
- [40] C. Reichhardt and C. Reichhardt, Directional locking effects for active matter particles coupled to a periodic substrate, *Phys. Rev. E* **102**, 042616 (2020).
- [41] W.-j. Zhu, W.-r. Zhong, J.-w. Xiong, and B.-q. Ai, Transport of particles driven by the traveling obstacle arrays, *J. Chem. Phys.* **149**, 174906 (2018).
- [42] Q. Chen and B.-q. Ai, Sorting of chiral active particles driven by rotary obstacles, *J. Chem. Phys.* **143**, 104113 (2015).
- [43] W. R. DiLuzio, L. Turner, M. Mayer, P. Garstecki, D. B. Weibel, H. C. Berg, and G. M. Whitesides, Escherichia coli swim on the right-hand side, *Nature (London)* **435**, 1271 (2005).
- [44] H. C. Berg and L. Turner, Chemotaxis of bacteria in glass capillary arrays. Escherichia coli, motility, microchannel plate, and light scattering, *Biophys. J.* **58**, 919 (1990).
- [45] B. M. Friedrich and F. Jülicher, Chemotaxis of sperm cells, *Proc. Natl. Acad. Sci.* **104**, 13256 (2007).
- [46] A. Cēbers, Diffusion of magnetotactic bacterium in rotating magnetic field, *J. Magn. Magn. Mater.* **323**, 279 (2011).
- [47] K. Ērglis, Q. Wen, V. Ose, A. Zeltins, A. Sharipo, P. A. Janmey, and A. Cēbers, Dynamics of magnetotactic bacteria in a rotating magnetic field, *Biophys. J.* **93**, 1402 (2007).
- [48] E. Lauga, W. R. DiLuzio, G. M. Whitesides, and H. A. Stone, Swimming in circles: Motion of bacteria near solid boundaries, *Biophys. J.* **90**, 400 (2006).
- [49] H. Löwen, Chirality in microswimmer motion: From circle swimmers to active turbulence, *Eur. Phys. J.: Spec. Top.* **225**, 2319 (2016).
- [50] L. Qin, M. J. Banholzer, X. Xu, L. Huang, and C. A. Mirkin, Rational design and synthesis of catalytically driven nanorotors, *J. Am. Chem. Soc.* **129**, 14870 (2007).
- [51] Y. Wang, S.-t. Fei, Y.-M. Byun, P. E. Lammert, V. H. Crespi, A. Sen, and T. E. Mallouk, Dynamic interactions between fast microscale rotors, *J. Am. Chem. Soc.* **131**, 9926 (2009).
- [52] J. Gibbs, S. Kothari, D. Saintillan, and Y.-P. Zhao, Geometrically designing the kinematic behavior of catalytic nanomotors, *Nano Lett.* **11**, 2543 (2011).
- [53] J. Gibbs and Y.-P. Zhao, Design and characterization of rotational multicomponent catalytic nanomotors, *Small* **5**, 2304 (2009).

- [54] See Supplemental Material at <http://link.aps.org/supplemental/10.1103/PhysRevE.105.054610> for videos and extra figures.
- [55] A. Nourhani, P. E. Lammert, A. Borhan, and V. H. Crespi, Kinematic matrix theory and universalities in self-propellers and active swimmers, *Phys. Rev. E* **89**, 062304 (2014).
- [56] A. Nourhani, V. H. Crespi, and P. E. Lammert, Gaussian memory in kinematic matrix theory for self-propellers, *Phys. Rev. E* **90**, 062304 (2014).
- [57] A. Nourhani, S. J. Ebbens, J. G. Gibbs, and P. E. Lammert, Spiral diffusion of rotating self-propellers with stochastic perturbation, *Phys. Rev. E* **94**, 030601(R) (2016).
- [58] J. G. Gibbs, A. Nourhani, J. N. Johnson, and P. E. Lammert, Spiral diffusion of self-assembled dimers of Janus spheres, *MRS Adv.* **2**, 3471 (2017).
- [59] P. Bayati and A. Nourhani, Memory effects in spiral diffusion of rotary self-propellers, *Phys. Rev. E* **105**, 024606 (2022).